Supplementary Information for

Unraveling the Transition from Alluaudite to Triphylite Phases during $LiFePO_4$ Hydrothermal Synthesis

Anna A. Kurashkina[1], Anastasia M. Alekseeva[1], Iana S. Soboleva[1,2], Alexey V. Sobolev[1,2], Andrey V. Mironov[1], Artem V. Marikutsa[1], Ivan V. Mikheev[1], Tatyana B. Shatalova[1], Igor A. Presniakov[1,2], Oleg A. Drozhzhin[1*], Evgeny V. Antipov[1]

[1]*Department of Chemistry, Lomonosov Moscow State University, 119991 Moscow, Russian Federation*
[2]*MSU-BIT University, Shenzhen, Guangdong Province 517182, P. R. China*

Inductively coupled plasma atomic emission spectrometry (ICP–AES) technique

Procedure 1. Digestion of the $LiFePO_4$ samples for the ICP–AES analysis.

The weighted portion of the sample (*ca*. 50 mg) of $Li_xFe_xP_xO_4$ was placed in a glass beaker of 100 ml. Concentrated HNO_3 (Panreac, Spain) was introduced in a volume of 45 ml, and subsequently heated at a temperature of 110℃ for a time span of 1 hour. Then *ca*. 15 ml of concentrated HCl acid (Panreac, Spain) was added and heated at 80℃ for 30 minutes to the getting yellowish clear solution. Solution put a volumetric flask (100.0 ml, class A) and deionized water added to the mark. Before conducting the analysis, all samples were diluted using deionized water at a ratio of 10:1 and 100:1.

ICP-AES operating parameters	
RF power, kW	1.3
Nebulizer gas flow rate, L/min	0.95
Auxiliary gas flow rate, L/min	1.5
Plasma gas flow rate, L/min	18
Sample flow rate, rpm	12
Integration time, s	25
Replicates	3
Wavelength, nm	
Li	460.289, 610.365
Fe	259.940, 238.204
P	213.618, 214.914
Sc (internal standard)	361.383

Procedure 2. Standards solutions preparation.

A standards reference solution of Li, Fe, and P (HPS, USA) was used. Stock solution 100 ppm was prepared and stabilized by 5 mass.% HNO_3. The solutions with concentrations ranging from 1 to 100 ppm were prepared as reference samples. A solution of Sc with a concentration of 20 ppm was employed as the internal standard. Additionally, Na_3PO_4 and $FePO_4{\times}2H_2O$ are used as extra quality control samples.

Analysis

The analysis was conducted using an Agilent 720 ICP-AES instrument. Liquid argon was employed to provide a source of argon gas. In this study, all necessary parameters, including nebulizer, auxiliary gas flow rates, RF power, and integration time, were optimized (refer to table 1). After analysis of each sample, the system was rinsed with 5 mass.% nitric acid for 10 s.

Two parallel samples were analyzed in all instances. The accuracy of the analysis was evaluated through the analysis of spiked samples. In accordance with the IUPAC Recommendations of 1994, all essential data was estimated using the prescribed nomenclature for presenting chemical analysis results.

Results

The assessment of the sample composition was conducted using ICP-AES data. It has been verified that there is no presence of sodium in the $LiFePO_4$ samples. The ICP data has verified that the $LiFePO_4$ chemical composition is in good agreement within the standard deviation and closely corresponds to the stoichiometric formula with good reproducibility. The presumed formulas for the three L11N19 samples are listed as follows:

- $Li_{0.98 \pm 0.02}Fe_{1.00 \pm 0.03}P_{0.98 \pm 0.02}$,
- $Li_{1.02 \pm 0.02}Fe_{0.98 \pm 0.02}P_{1.00 \pm 0.02}$,
- and $Li_{1.00 \pm 0.02}Fe_{1.03 \pm 0.02}P_{1.00 \pm 0.01}$.

For Na-containing samples (designated as $Na_{0.7}Fe_3(HPO_4)_2(PO_4)$ and $Na_{1.8}Fe_3(PO_4)_3$), the composition is the following: $Na_{0.74 \pm 4}Fe_{3.04 \pm 15}P_{2.94 \pm 15}$ and $Na_{1.83 \pm 0.09}Fe_{2.99 \pm 0.15}P_{2.94 \pm 0.15}$.

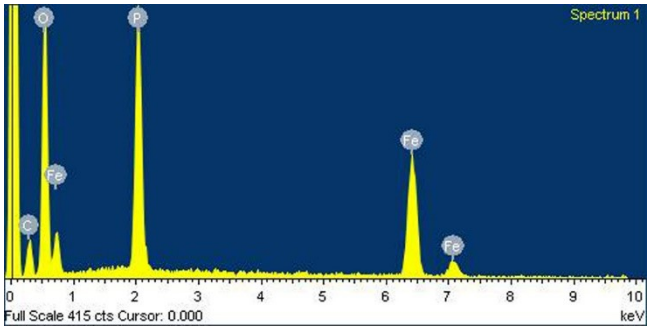

Fig. S1. EDX spectrum of synthesized sample of LFP (L11N19).

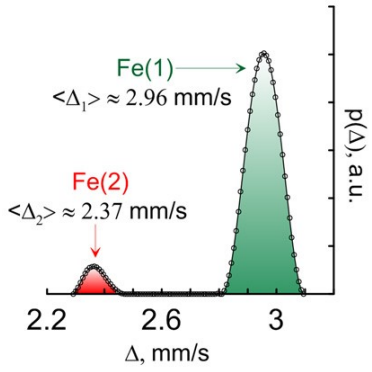

Fig. S2. The *p*(*Δ*) distribution and its representation as the superposition of normal distributions corresponding to crystal sites of ^{57}Fe probe nuclei within M1 and M2 sites (the average values $<\Delta_i>$ are indicated).

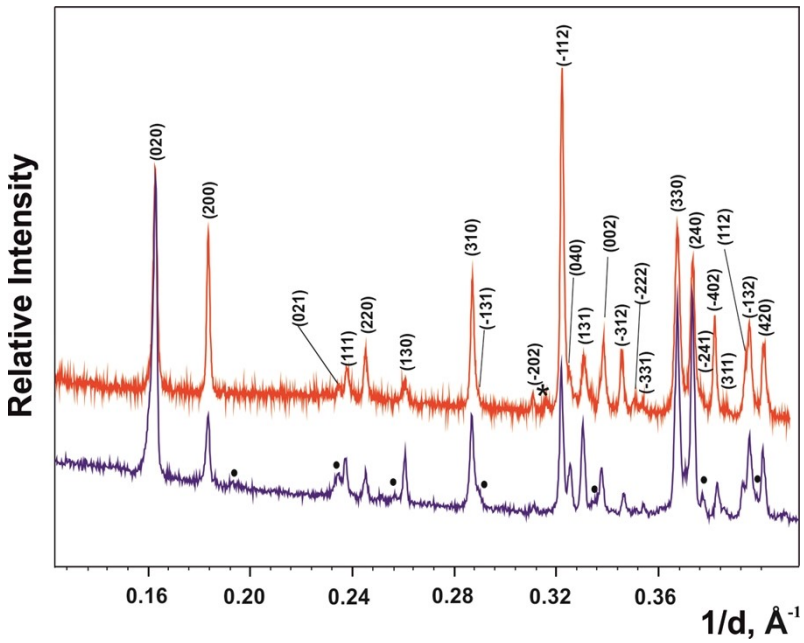

Fig. S3. PXRD patterns of the synthesized sodium iron alluaudite phase $Na_{0.7}Fe_3(HPO_4)_2(PO_4)$ (*top, red*) and the probe taken 1 h later during the synthesis of L11N19 sample (*bottom, blue*). The diffraction maxima are indexed in sp.gr *C* 2/*c* with the lattice parameters: *a* = 11.9917(8) Å, *b* = 12.3080(9) Å, *c* = 6.4995(4) Å, β = 114.554(2)°. The reflections of $LiFePO_4$ are marked by «●».

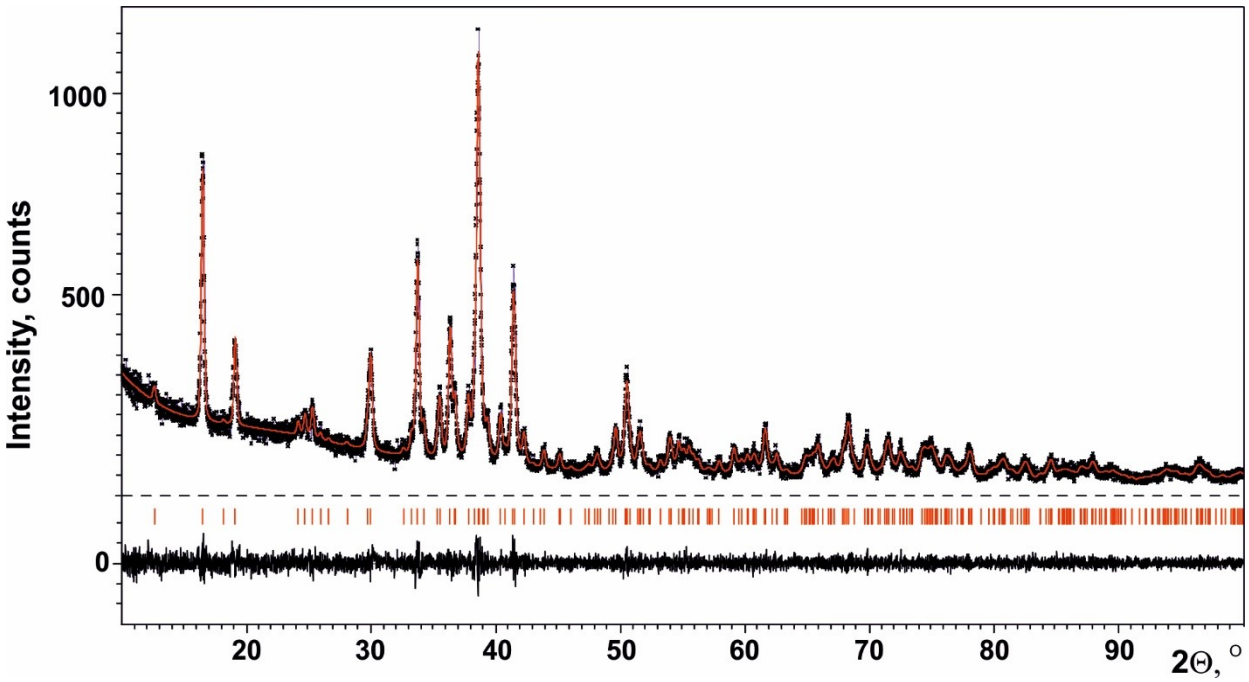

Fig. S4. Results of the full profile Le Bail refinement of PXRD pattern (λ = Co$K_{\alpha 1}$) of the $Na_{1.8}Fe_3(PO_4)_3$ sample: sp. gr. *C*2/*c*, *Z* = 4, *a* = 11.8827(3) Å, *b* = 12.5337(9) Å, *c* = 6.4504(3) Å , β = 114.399(5) °, V = 874.9(1) Å^3, R_p = 0.072, R_{wp} = 0.093, GOF = 1.03.

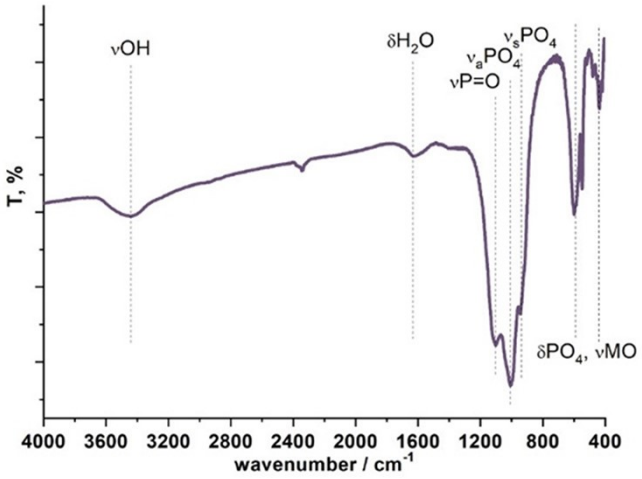

Fig. S5. FTIR spectrum for the $Na_{1.8}Fe_3(PO_4)_3$ sample.

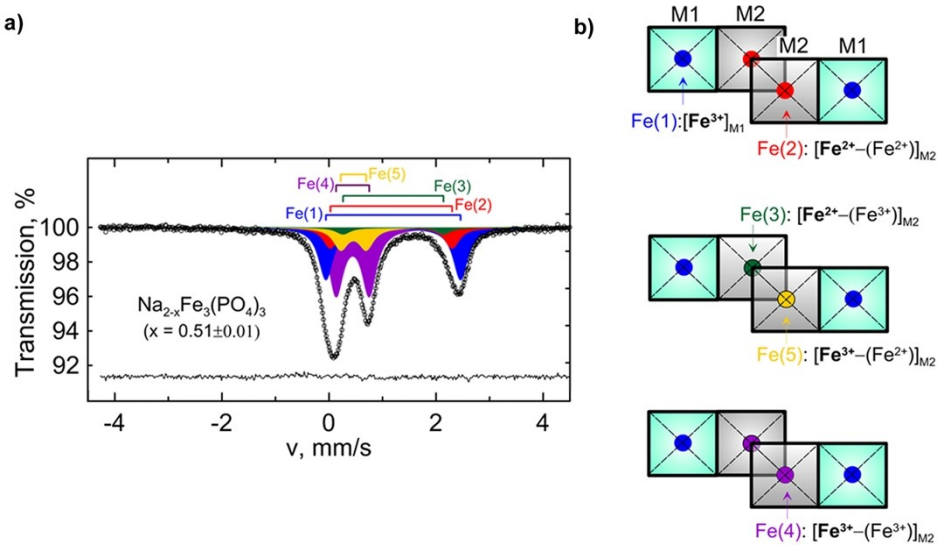

Fig. S6. ^{57}Fe Mössbauer spectrum for the $Na_{1.8}Fe_3(PO_4)_3$ sample recorded at RT **(**a), the four different configurations of the next-nearest neighbor M2 sites occupied by Fe^{3+} and Fe^{2+} (b) (see text).

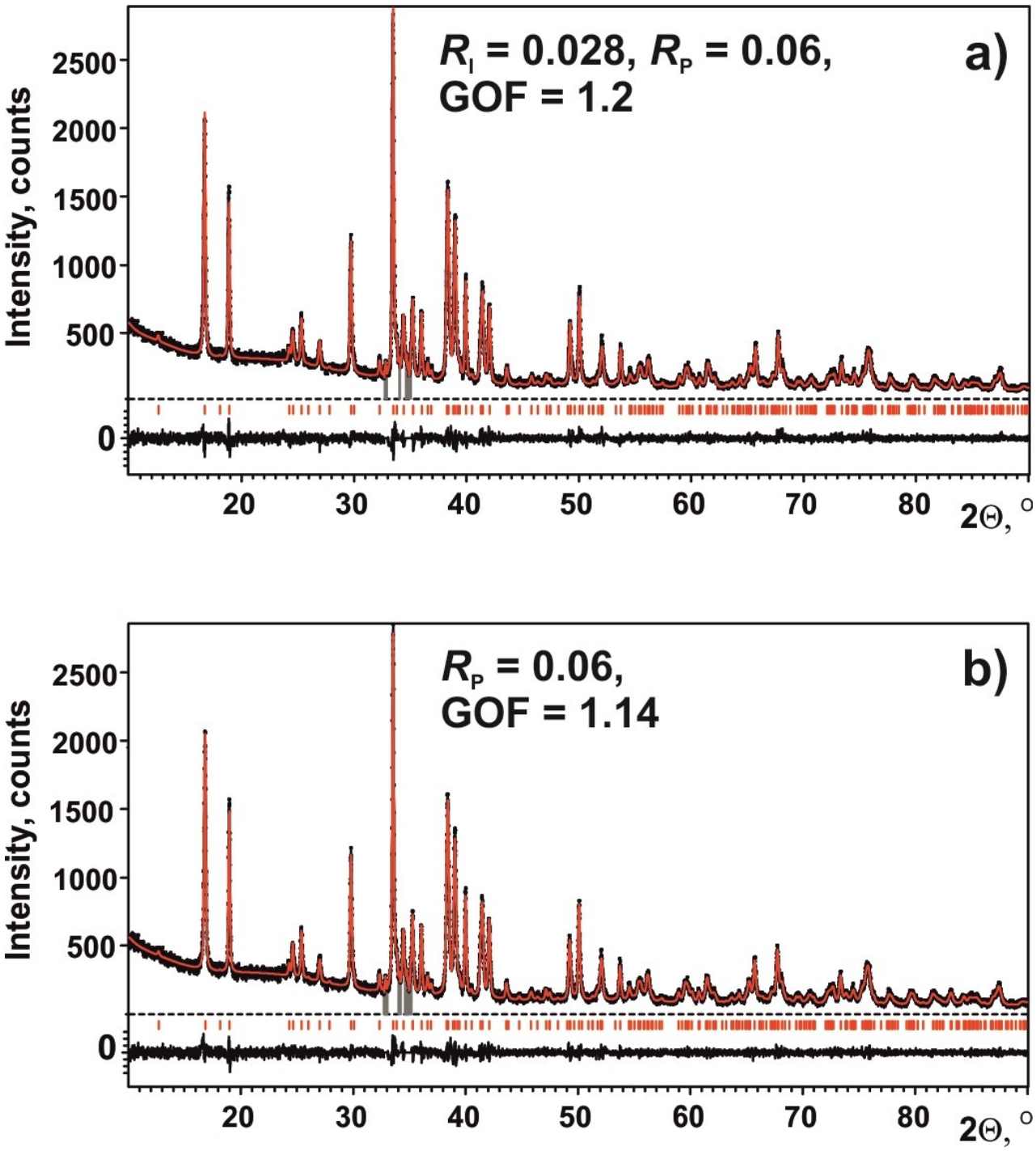

Fig. S7. Results of refinement by Rietveld method (a) and full profile refinement by Le Bail method (b) of the PXRD data of $Na_{0.7}Fe_3(HPO_4)_2(PO_4)$ with the corresponding values of the reliability factors.

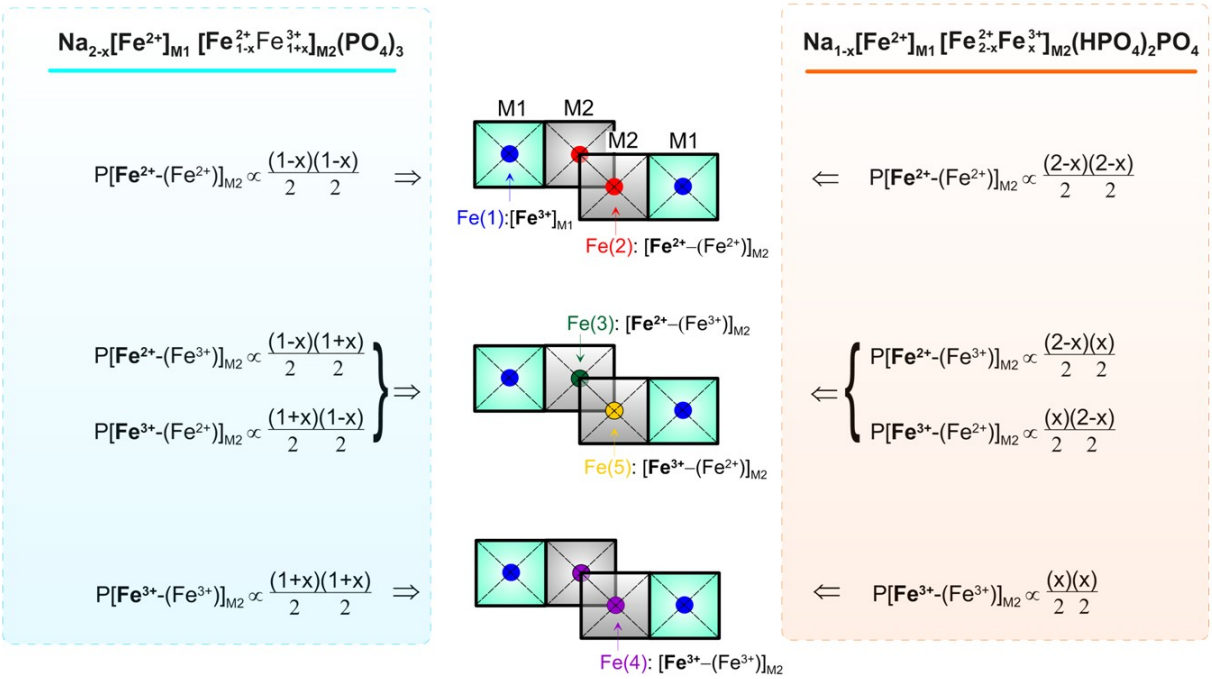

Fig. S8. The four different configurations and their probabilities (P) of the next-nearest neighbor M2 sites occupied by Fe^{3+} and Fe^{2+} in $Na_{1.8}Fe_3(PO_4)_3$ (*left panel*) and $Na_{0.7}Fe_3(HPO_4)_2(PO_4)$ (*right panel*)

Table S1. Selected interatomic distances for $Na_{0.7}Fe_3(HPO_4)_2(PO_4)$.

Atoms	Distance, Å	Atoms	Distance, Å
Na–O6 × 2	2.30(1)	P1–O1 × 2	1.55(2)
O6 × 2	2.43(2)	O2 × 2	1.56(2)
O3 × 2	2.84(3)		
Fe1–O3 × 2	2.14(2)	P2–O4	1.54(2)
O6 × 2	2.18(2)	O5	1.54(2)
O3 × 2	2.23(2)	O6	1.54(2)
		O3	1.57(2)
Fe2–O6	2.06(2)	H – O2	0.90(12)
O5	2.07(2)	O4 × 2	2.36(15)
O3	2.11(2)		
O2	2.12(2)		
O1	2.13(2)		
O5	2.18(5)		

Table S2. Bond valence sums for $Na_{0.7}Fe_3(HPO_4)_2(PO_4)$.

Atom	BVS
Na	0.97
Fe1	1.88

Fe2	2.19
P1	4.86
P2	4.85
O1	1.90
O2	2.6
O3	1.92
O4	1.57
O5	1.98
O6	1.92
H	1.2

Mössbauer spectroscopy (MS) technique for alluadite-type $Na_{0.7}Fe_3(HPO_4)_2(PO_4)$ and $Na_{1.8}Fe_3(PO_4)_3$

The fit of Mössbauer spectrum for $Na_{2-x}Fe_3(PO_4)_3$ shown in Fig. S6a is based upon a binomial distribution of nearest-neighbor environments of iron on the M2 sites resulting from a random distribution Fe^{2+} and Fe^{3+} ions on the adjacent M2 sites. Such a binomial distribution has been used earlier to fit the ^{57}Fe Mössbauer spectra of alluaudite-like minerals $Na_2Mn_{2-x}Fe_{1+x}(PO_4)$ [S1-S5]. It was assumed that the M1 sites are fully occupied by Fe^{2+} ions [Fe(1) subspectrum] because of their larger ionic radius. According to this model, four different next-nearest neighbor iron environments are possible (Fig. S6b) giving two Fe^{2+} [Fe(2), Fe(3)] and two Fe^{3+} [Fe(4), Fe(5)] quadrupole doublets. Small variations in the redox conditions during synthesis can lead to oxidation of Fe^{2+} to Fe^{3+}, which is coupled with partial replacement of Na^+ by vacancies (V_{Na}) due to charge compensation mechanism: $\mathrm{Na}^{x}_{Na(M2)} + \mathrm{Fe}^{x}_{Fe(M2)} \rightarrow \mathrm{V}^{/}_{Na(M2)} + \mathrm{Fe}^{\bullet}_{Fe(M2)}$. Taking (1+x)/3 and (2−x)/3 as Fe^{3+} and Fe^{2+} fractions in the M2 sites in $\mathrm{Na}_{2-x}[\mathrm{Fe}^{2+}]_{M1}[\mathrm{Fe}^{2+}_{2-x}\mathrm{Fe}^{3+}_{1+x}]_{M2}(\mathrm{PO}_4)_3$, the probabilities (*P*) for the four different iron environments in the M2 site were obtained (Fig. S8). Mössbauer spectral hyperfine parameters for the five iron sites are presented in Table S5. The fraction x ≈ 0.51 obtained from Mössbauer spectrum appears to be substantially larger than that obtained by ICP-AES and PXRD refinement analysis that give x ≈ 0.2. This may indicate the presence of oxidized surface layers, amorphous phases and/or internal defects typical of materials synthesized under hydrothermal conditions.

We used a similar fitting procedure for Mössbauer spectrum of $Na_{1-x}Fe_3(HPO_4)_2PO_4$ (Fig. 3d). The value of sodium non-stoichiometry (x) was used as one of the variable parameters of the spectrum, through which the probabilities of various local configurations in the iron environment were expressed (Fig. S8). Mössbauer spectral hyperfine parameters for the five iron sites are presented in Table S4. As in the case of the $Na_{2-x}Fe_3(PO_4)_3$ sample, there is a deviation of the x ≈ 0.50 value obtained from the

spectrum from the corresponding value x ≈ 0.3 independently determined from ICP-AES analysis and PXRD refinement. The reasons are most probably the same.

The decrease in temperature (300 K → 77 K) resulted in two expected changes: (i) an increase in the isomer shift of all components (Table S6), due to the second-order Doppler effect, (ii) and a sharp increase in quadrupole splitting for the partial spectra of divalent iron Fe(1), Fe(2) and Fe(3). The change in the relative positions of some components of the doublets Fe(i) (Fig. S9) is associated with different temperature dependences of the quadrupole splittings corresponding to iron cations in different crystal positions (different local environments). It is important to note that a decrease in temperature leads to a decrease in the total area of the divalent iron spectra ($A_{Fe(II),\ 300K}$ = 83.1% → $A_{Fe(II),\ 77K}$ = 73.6%), thereby confirming our assumption about the ratio of effective Debye temperatures $\Theta_{Fe(II)} > \Theta_{Fe(III)}$. Thus, the difference in the Lamb-Mössbauer factors cannot explain the discrepancy between the Mössbauer spectra and atomic emission spectroscopy data.

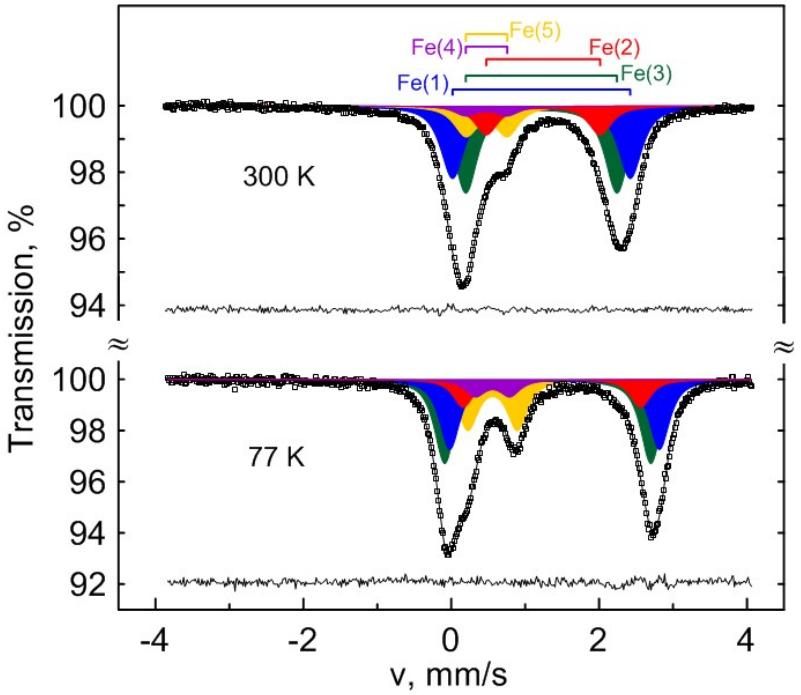

Fig. S9. ^{57}Fe Mössbauer spectra for the $Na_{0.7}Fe_3(HPO_4)_2(PO_4)$ sample recorded at RT and 77 K

Table S3. Hyperfine parameters of the ^{57}Fe Mössbauer spectra for $LiFePO_4$ (L11N19) sample at RT.

Component	Valence State	δ, mm/s	Δ, mm/s	W, mm/s (*)	***A***, %
Fe(1)	$[Fe^{2+}]_{M2}$	1.22(1)	2.95(1)	0.27(1)	91.1(2)
Fe(2)	$[Fe^{2+}]_{M1}$	1.19(1)	2.31(2)	0.27(1)	5.9(8)
Fe(3)	$[Fe^{3+}]_{M1/M2}$	**0.49(1)**	0.42(2)	0.27(1)	3.0(8)

(*) *W* is the full width at half-maximum (corresponding values were considered equal to each other).

Table S4. Hyperfine parameters of the ^{57}Fe Mössbauer spectra for $Na_{0.7}Fe_3(HPO_4)_2(PO_4)$ at RT.

Component	Site and local surrounding	δ, mm/s	Δ, mm/s	*W*, mm/s (*)	***A***, %
Fe(1)	$[\mathbf{Fe^{2+}}]_{M1}$	1.22(1)	2.40(1)	0.38(1)	32.0(2)
Fe(2)	$[\mathbf{Fe^{2+}}–(Fe^{3+})]_{M2}$	1.24(1)	1.54(1)	0.38(1)	12.7(1)
Fe(3)	$[\mathbf{Fe^{2+}}–(Fe^{2+})]_{M2}$	1.22(1)	1.04(1)	0.38(1)	38.4(3)
Fe(4)	$[\mathbf{Fe^{3+}}–(Fe^{3+})]_{M2}$	0.47(1)	0.56(1)	0.38(1)	4.2(2)
Fe(5)	$[\mathbf{Fe^{3+}}–(Fe^{2+})]_{M2}$	0.47(1)	0.56(2)	0.38(1)	12.7(2)

(*)*W* is the full width at half-maximum (corresponding values were considered equal to each other).

Table S5. Hyperfine parameters of the ^{57}Fe Mössbauer spectra for $Na_{1.8}Fe_3(PO_4)_3$ sample at RT.

Component	Site and local surrounding	δ, mm/s	Δ, mm/s	*W*, mm/s (*)	***A***, %
Fe(1)	$[\mathbf{Fe^{2+}}]_{M1}$	1.20(1)	2.51(1)	0.33(1)	31.4(2)
Fe(2)	$[\mathbf{Fe^{2+}}–(Fe^{3+})]_{M2}$	1.17(1)	2.27(1)	0.33(1)	12.7(1)
Fe(3)	$[\mathbf{Fe^{2+}}–(Fe^{2+})]_{M2}$	1.20(1)	1.87(1)	0.33(1)	4.0(2)
Fe(4)	$[\mathbf{Fe^{3+}}–(Fe^{3+})]_{M2}$	0.44(1)	0.62(1)	0.33(1)	39.3(3)
Fe(5)	$[\mathbf{Fe^{3+}}–(Fe^{2+})]_{M2}$	0.46(1)	0.48(1)	0.33(1)	12.6(1)

(*)*W* is the full width at half-maximum (corresponding values were considered equal to each other).

Table S6. Hyperfine parameters of the ^{57}Fe Mössbauer spectra for $Na_{0.7}Fe_3(HPO_4)_2(PO_4)$ at 77 K.

Component	Site and local surrounding	δ, mm/s	Δ, mm/s	*W*, mm/s (*)	*A*, %
Fe(1)	$[\mathbf{Fe^{2+}}]_{M1}$	1.40(1)	2.84(1)	0.33(1)	28.3(3)
Fe(2)	$[\mathbf{Fe^{2+}}–(Fe^{3+})]_{M2}$	1.36(1)	2.40(1)	0.33(1)	11.3(2)
Fe(3)	$[\mathbf{Fe^{2+}}–(Fe^{2+})]_{M2}$	1.31(1)	2.74(1)	0.33(1)	34.1(3)
Fe(4)	$[\mathbf{Fe^{3+}}–(Fe^{3+})]_{M2}$	0.56(2)	0.57(1)	0.33(1)	6.5(4)

Fe(5)	[**Fe^{3+}**–(Fe^{2+})]$_{M2}$	0.47(1)	0.56(2)	0.33(1)	19.8(2)

(*)*W* is the full width at half-maximum (corresponding values were considered equal to each other).

References

S1. Hatert, Frédéric, Hermann, Raphaël P., Long, Gary J., Fransolet, André-Mathieu and Grandjean, Fernande. "An X-ray Rietveld, infrared, and Mössbauer spectral study of the NaMn($Fe_{1-x}In_x$)$_2$(PO_4)$_3$ alluaudite-type solid solution" American Mineralogist, vol. 88, no. 1, 2003, pp. 211-222. https://doi.org/10.2138/am-2003-0124

S2. Hatert, Frédéric, Rebbouh, Leila, Hermann, Raphaël P., Fransolet, André-Mathieu, Long, Gary J. and Grandjean, Fernande. "Crystal chemistry of the hydrothermally synthesized $Na_2(Mn_{1-x}Fe_x^{2+})_2Fe^{3+}(PO_4)_3$ alluaudite-type solid solution" American Mineralogist, vol. 90, no. 4, 2005, pp. 653-662. https://doi.org/10.2138/am.2005.1551

S3. Hatert, F., Long, G., Hautot, D. et al. A structural, magnetic, and Mössbauer spectral study of several Na–Mn–Fe-bearing alluaudites. Phys Chem Minerals 31, 487–506 (2004). https://doi.org/10.1007/s00269-004-0400-4

S4. Raphaël P. Hermann, Frédéric Hatert, André-Mathieu Fransolet, Gary J. Long, Fernande Grandjean, Mössbauer spectral evidence for next-nearest neighbor interactions within the alluaudite structure of $Na_{1-x}Li_xMnFe_2(PO_4)_3$, Solid State Sciences, Volume 4, Issue 4, , April 2002, Pages 507-513, https://doi.org/10.1016/S1293-2558(02)01278-5

S5. Redhammer, Günther J.; Tippelt, Gerold; Bernroider, Manfred; Lottermoser, Werner; Amthauer, Georg; Roth, Georg, Hagendorfite (Na,Ca)$MnFe_2(PO_4)_3$ from type locality Hagendorf (Bavaria, Germany): crystal structure determination and 57Fe Mossbauer spectroscopy, European Journal of Mineralogy Volume 17 Number 6 (2006), p. 915 - 932, https://doi.org/10.1127/0935-1221/2005/0017-0915